E18-2006-66

Yu. V. Taran, J. Schreiber[1], U. Stuhr[2], H. Kockelmann[3],
A. M. Balagurov, V. B. Zlokazov

RESIDUAL STRESSES IN A COMPOSITE STEEL TUBE
MEASURED BY NEUTRON DIFFRACTION

[1] Fraunhofer Institute for Nondestructive Testing (Dresden branch), Germany
[2] SINQ, Paul Scherrer Institute, Switzerland
[3] MPA, Stuttgart University, Germany

Таран Ю. В. и др.   Е18-2006-66

Измерение остаточных напряжений в композитной стальной трубе
методом нейтронной дифракции

Пространственное распределение остаточных внутренних напряжений в композитной трубе из аустенитной нержавеющей стали с внешней наварной плакировкой из ферритной стали было измерено методом неразрушающей времяпролетной нейтронной дифракции на стресс-дифрактометре POLDI на импульсном источнике PSI SINQ. Проведено сравнение результатов нейтронных измерений с данными, полученными разрушающим методом контроля напряжений путем обтачивания трубы и высверливания калибровочных отверстий, а также с результатами расчетов методом конечных элементов. Только для тангенциальной компоненты тензора напряжений было получено полуколичественное согласие между результатами всех использованных методов. Наблюдалось заметное расхождение в результатах этих методов для аксиальной компоненты. Малость радиальной компоненты была показана всеми методами, однако с некоторым различием в ее пространственном распределении.

Работа выполнена в Лаборатории нейтронной физики им. И. М. Франка ОИЯИ.

Taran Yu. V. et al.   E18-2006-66

Residual Stresses in a Composite Steel Tube Measured by Neutron Diffraction

The triaxial residual stresses in a composite tube from an austenitic stainless steel with a welded ferritic steel cladding were measured by the time-of-flight neutron diffraction method on the POLDI instrument at the PSI SINQ facility. The POLDI results are compared to the results obtained by the destructive turning out method and theoretical predictions of calculations by the finite element method. Only for the tangential component of the stress tensor the semiquantitative agreement of all used methods was observed. There is a clear discrepancy between the results of the different methods in the axial component. For the radial component all methods reveal quite small stresses, however, with some distinct differences in their distributions.

The investigation has been performed at the Frank Laboratory of Neutron Physics, JINR.

1. BACKGROUND

Compared to carbon and alloy steels, all corrosion resistant alloys are expensive. In many cases, corrosion resistance is required only on the surface of the material and carbon or alloy steel can be clad with a more corrosion resistant alloy. Cladding can save up to 80% of the cost of using solid alloy. Cladding of carbon or low alloy steel can be accomplished in several ways including roll bonding, explosive bonding, weld overlaying and «wallpapering». Clad materials are widely used in chemical processes, offshore oil production, oil refining and electric power generation industries. Weld overlaying is commonly used to clad the surfaces of fabricated steel structures. However, the existence of uncontrollable residual stress distributions in welded materials prevents this method from being widely applied.

In a particular case, shape welded ferritic layers on austenitic tubes can help us to suppress stress corrosion because these layers produce the compressive stress states on the austenitic tube. The analysis of residual stresses through the ferritic weld into the austenitic material can be helpful for the optimization of the corresponding welding overlaying technique.

For the first time, we have investigated such a composite steel tube by the non-destructive neutron diffraction (ND) method on the HRFD instrument at the IBR-2 pulsed reactor [1]. But because of the limited beam time we have only measured two of three components of the residual strain tensor. To restore the full residual stress tensor we have repeated the experiment on the ENGIN instrument at the ISIS pulsed facility [2]. However, in both experiments we have experienced difficulties in determining the stress free references for calculating the residual strains. Also some uncertainty in residual strain determination was introduced due to the absence of strain state control at the last stage of a sample preparation (Fig. 1). Nevertheless, in both experiments we have observed a qualitative agreement between the calculation results of difference of the radial and tangential stress tensor components and the data obtained by the turning out method (TOM), the destructive ring core method (RCM), as well as those of the theoretical predictions of calculations by the finite element method (FEM). Details of the TOM and RCM measurements, as well as the FEM calculation are given in [3].

Taking into account these circumstances together with a recently developed new technique for stress free references (comb samples) [4–6], we have carried

out the third experiment on the POLDI stress-diffractometer at the PSI SINQ facility with better-formed geometry of the sample from the composite steel tube supplementing it with measurements using a comb sample. In the basis of the comb technique there is an idea that the teeth of the comb sample are strain-relieved zones and that the residual strains can be fully relieved at the ends of the teeth yielding the strain-free lattice parameters. Note, however, that this relief relates only to macrostresses (the stress of the I type). The effects of inter-granular microstresses (the stress of the II type) and microstructure are in principal left. To our knowledge, a first application of the comb-sample technique is described in [4].

In this paper, the results of the last measurements of the stress state with the composite steel tube on the POLDI stress-diffractometer are presented. New results have allowed us to determine correctly the triaxial distribution of the residual stresses and compare them to the data obtained in the previous experiments and also to TOM, RCM and FEM results.

2. EXPERIMENTAL DETAILS

Samples. To fabricate the composite steel tube seven layers of ferritic steel with 135 welding traces and a total length of 1100 mm were welded on a 15 mm thick austenitic steel tube with an outer radius of 148 mm. The outer radius of the manufactured two-layer tube was 168 mm. The chemical composition of the layers is given in Table 1. Most parameters of materials, including elastic constants, tensile strength, and hardness were obtained by cutting test specimens. Austenitic steel was found to have $E = 176$ GPa, $\nu = 0.3$, $R_m = 536$ MPa and the hardness 155 HV10. For a ferritic welded material, the average values $E = 205$ GPa, $\nu = 0.3$, $R_m = 695$ MPa and the hardness 200 HV10 far from the transition region, where its value reaches 380 HV10, were found.

Table 1. The chemical composition of the layers in the composite tube

Layer	Steel	C	Si	Mn	P	S
Inner layer (austenite, γ phase)	X6CrNiTi 18 10	0.06	0.44	1.77	0.031	0.003
Outer layer (ferrite, α phase)	3NiMo 1UP	0.06	0.12	1.03	0.021	0.004

Cr	Ni	Mo	V	Al	Cu	W	Co	Ti
17.0	10.6	0.34	0.07	0.20	0.32	0.05	0.12	0.39
0.52	1.02	0.57	< 0.01	0.01	0.06	< 0.01	0.03	< 0.01

For measurements at neutron sources, the same samples were prepared (Figs. 1 and 2). First, the 200 mm long tube was cut from the manufactured

2

tube (Fig. 1, *a*). Then a 70° of arc circumference segment was truncated from the 200 mm long tube (Fig. 1, *b*). With the extensometers placed in the middle of the segment oriented in the axial and circumferential (tangential) directions, the
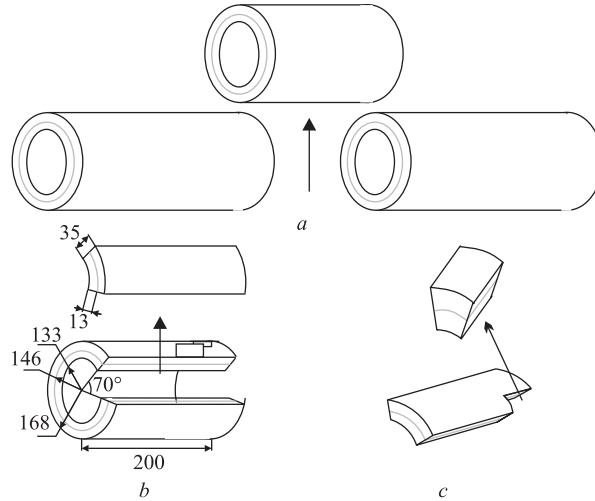

Fig. 1. Preparation scheme of the sample for measurements at the IBR-2 and ISIS facilities: *a* — cutting out the 200 mm long tube, *b* — cutting out the 70° circumference segment, *c* — cutting out the main sample from the segment

effect of stress release was measured at the inner and outer surfaces (see Table 2). This release has to be accounted for a recalculation of segment experimental data as applied to the whole tube. The sample investigated at the IBR-2 and ISIS facilities was cut out from the 70° circumference segment in the form of a smaller segment as shown in Fig. 1, *c*. A small stress release was possible during the last stage of cutting but it was not controlled with any stress gages.

Table 2. Stress release results for the truncated tube segment

Strain/ Stress	Inner side		Outer side	
	Axial	Tangential	Axial	Tangential
$\Delta\varepsilon$ [10^{-6}]	–274(20)	2130(4)	427(10)	–1526(9)
$\Delta\sigma$ [MPa]	–80 (4)	–450 (2)	6 (3)	307 (2)

To prepare the samples for measurements on the POLDI stress-diffractometer we have cut out two 10 mm thick slices from the 70° circumference segment. One slice was used as the main sample for measurements of the radial (Fig. 2), axial and tangential (hoop) components of the strain tensor. From another slice (Fig. 3, left) we have made three small samples of 10 mm thick (Fig. 3, right)

3

using electro-discharge machining (EDM): 1) the comb sample 1 with teeth of 1.5 mm width along the radial direction, at that, their width along the axial direction equals to the sample's size in the same direction; 2) the comb sample 2 with teeth of 3 mm width; 3) the sample 3 without the teeth. All teeth had a height of 8.5 mm, thus, support for the teeth had a thickness of 1.5 mm. The width of slits between teeth was 0.3 mm. Some other data on the comb samples are submitted in Table 3.
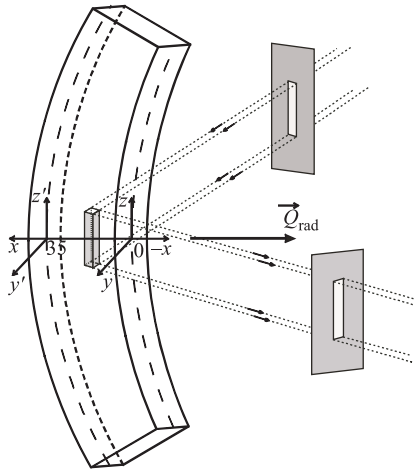

Fig. 2. Main sample in a position for measurements in the radial direction
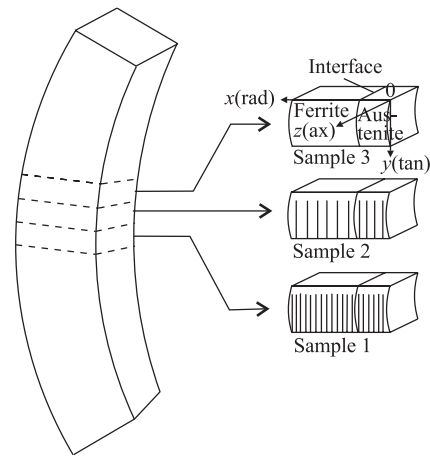
Fig. 3. Sheme of preparation of small samples from the 70° curcumference segment slice

Table 3. Comb samples from the composite tube

Comb sample	Tooth width, mm	Number of teeth in phase		Interface location
		Austenite	Martensite	
1	1.5	1–6	8–20	tooth 7
2	3	1–4	6–11	tooth 5

POLDI set-up. The POLDI instrument is the high intensity, high resolution multiple pulse overlap time-of-flight stress-diffractometer at the SINQ neutron source. The high intensity is achieved by allowing frame-overlap. The angular information, usually not used by time-of-flight diffractometers, allows the reconstruction of the diffraction pattern from the multiple pulse-spectrum.

The POLDI diffractometer consists of some major components (Fig. 4): the collimator of direct neutron beam, the $xyz\omega$ positioner, the secondary radial multislit collimator and the neutron detector. The basic table of the positioner
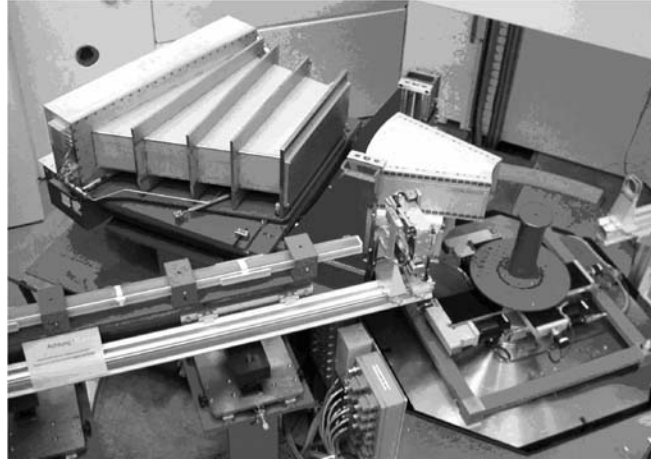
4

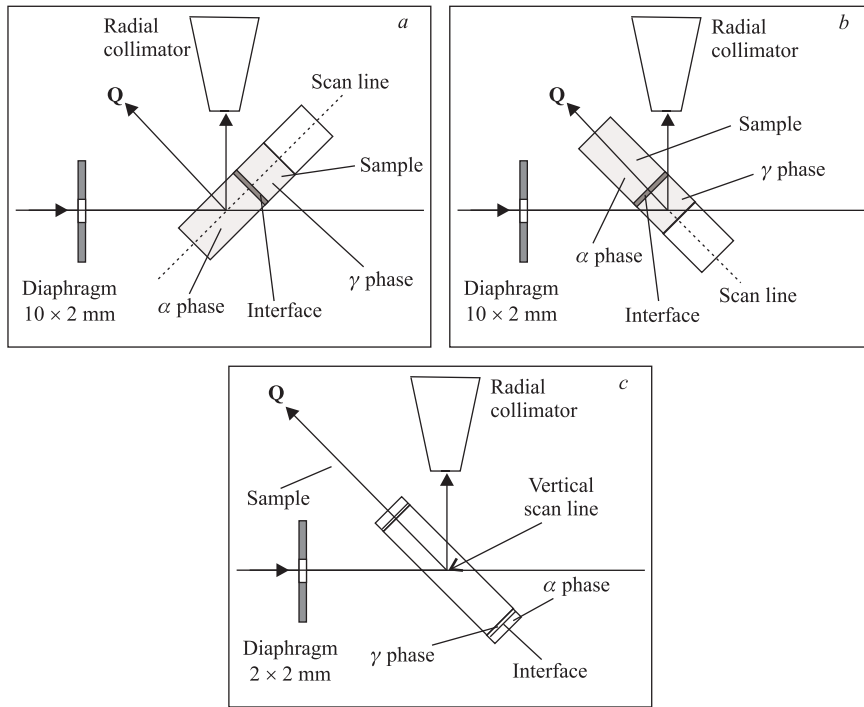Fig. 4. The POLDI stress-diffractometer

Fig. 5. Measurements with the main sample in the direction: a — axial, b — radial, c — hoop

5

has a load capacity of 10 t. It can be moved vertically in a range of 520 mm. On this table different sample tables can be mounted. Usually a rotation table is mounted. The rotation centre of the table is aligned to the centre of the gauge volume. The rotation table can be driven in a range of ± 180°. On this rotation table two perpendicular linear tables are installed. The movement range for both units is ± 150 mm. The load capacity of this positioning system is 200 kg. The samples can be fixed at three plates differing in their diameters. For large and heavy specimens a big plate with a diameter of 490 mm can be used. An incoming beam slit definition system consists of a motorized translation stage carrying a frame supporting the motorized slits forming a square or rectangular aperture. The translation table can be driven from its home position to software limited position close to the sample.

Sample positions and scanning regime. The measurements were started at the radial orientation position of the main sample (Figs. 2 and 5, c). The gauge volume inside samples was formed a diaphragm into the primary neutron beam and the radial collimator with the space resolution of 2 mm in the scattering beam, respectively. For measuring the radial and axial components, height and width of the diaphragm were equaled to 10 and 2 mm, respectively (Fig. 2). For the axial measurements the sample was turned on 90° around the vertical axis by a drive motor (Fig. 5, b).

Upon completing the axial measurements, the sample was turned manually into a position shown in Fig. 5, a. In this case the height of the diaphragm was decreased up to 2 mm. Strain scanning of the sample was done at the depth of 5 mm from the surface along the radial direction of the composite tube begun from $x = 2$ mm and finished at $x = 34$ mm where coordinates $x = 0$ and 35 mm correspond to the inner and outer edges of the tube, respectively. The scan step was equal to 1 mm in the austenite (γ phase) part of the sample and in the ferritic (α phase) part close to the interface between austenitic and ferritic layers of the tube while the step was equal to 2 mm in the ferritic part far off the interface.

The measurements with the comb sample 2 (teeth of 3 mm width) were done only in the radial and axial directions due to a limitation on the neutron beam time. The measurements with the comb sample 1 (teeth of 1.5 mm width) were impossible because of the insufficient space resolution of the used radial collimator.

Data processing. The initial processing of the measured spectra was carried out using the in-house single peak fit program «Poldiausfit» which determined positions of the selected diffraction peaks in the d-spacing. Eight and seven resolved single peaks were observed in the austenite and ferrite phases, respectively. An example of the single peak fit spectra obtained in the ferrite part of the composite tube at $x = 34$ mm is shown in Fig. 6. Using a set of the selected peak positions we have calculated the lattice parameter for each spectrum by applying the autoindexing program «Autox» created at FLNP JINR [7].
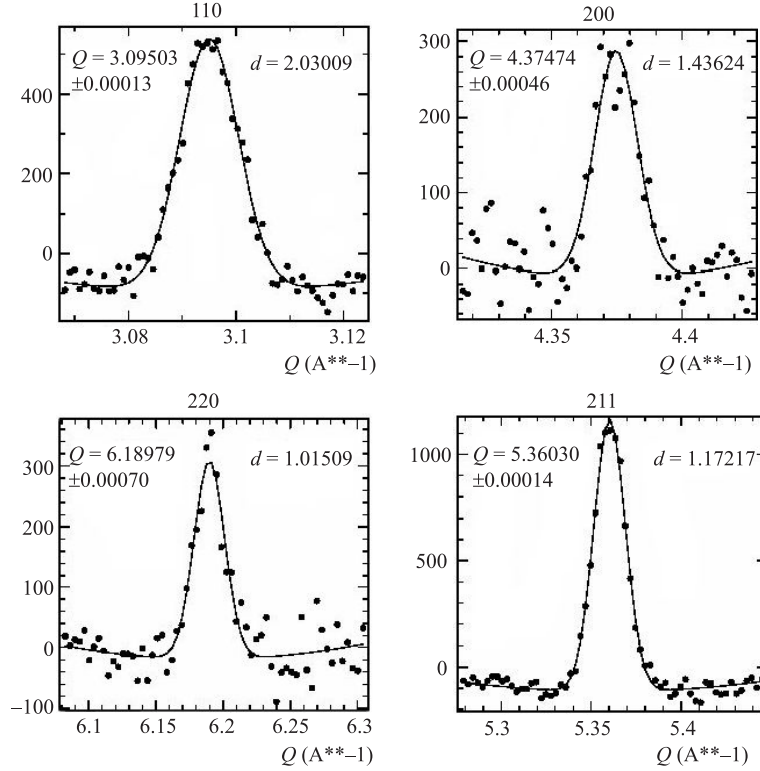
Fig. 6. Single peak fit of the ferrite spectra obtained close to the tube edge

3. EXPERIMENTAL RESULTS

3.1. Main sample. Parent tube (austenite). In Fig. 7, we have presented the dependences of the austenite phase lattice parameter of the main sample obtained from results of the single peak fitting and the autoindexing on the location x of the gauge volume along the tube radius for the radial, axial and tangential directions of the scattering vectors. Note practical absence of the lattice parameter variation in the radial and tangential directions. A noticeable growth of the lattice parameter in the axial direction was observed close to the interface.

The austenite phase texture and the microstresses of the III type are characterized by Figs. 8 and 9, where the dependences of the intensity and the full width on half maximum (FWHM) of the selected peaks on the location x of the gauge volume are shown for all three scattering vector directions. Note that the peaks width weakly depends on the coordinate x while the intensity of the
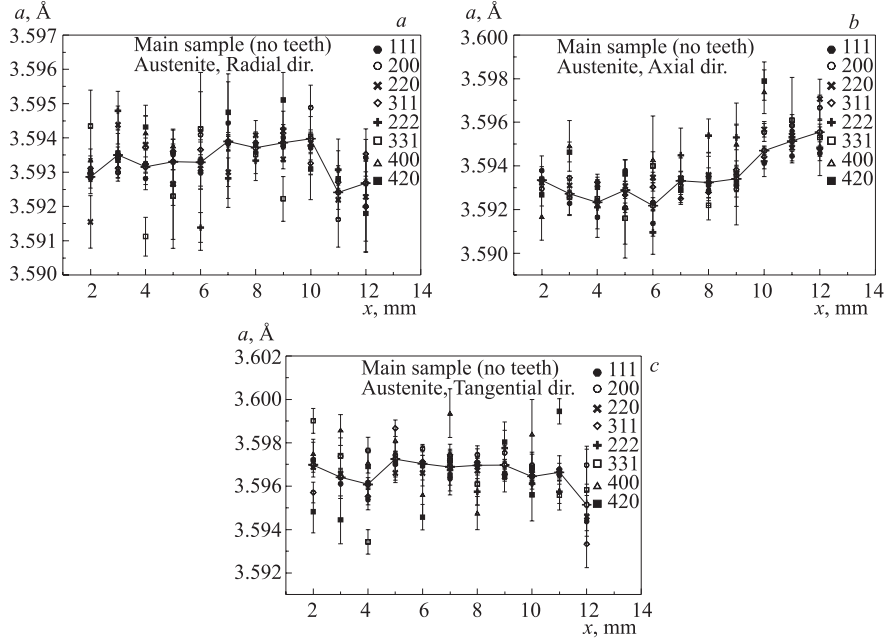
7

Fig. 7. Lattice parameters of the austenite phase of the main sample on the location x of the gauge volume in the direction: a — radial, b — axial, c — tangential

peaks strongly vary through the austenite phase, especially, the reflex (200) for the radial direction and the reflex 311 for the axial direction.

To clarify the role of the grain interaction stresses (the microstresses of the II type) the character of the dependence of the lattice parameter on the anisotropy factors G was investigated. In the case of the cubic lattice, the orientation factor is $G = (h^2k^2 + h^2l^2 + k^2l^2)/(h^2 + k^2 + l^2)^2$. As seen from Fig. 10, the lattice parameters vary nonlinearly. It points to the presence of the visible grain interaction stresses. Unfortunately, this circumstance causes some difficulties in the analysis of the macroscopic stress state, i. e., the residual macrostresses of the I type are difficult to be extracted in this case.

However, the more attentive analysis of behavior of the anisotropy curves (Fig. 10) shows that the scattering of the experimental points is less near to the inner edge of the austenite part than near to the austenite-ferrite interface. At that, the anisotropy curves are more closely grouped in the coordinate interval of $x = $ 2–6 mm. For the radial direction, the grouped curves do not on average have the evident slope that points on smallness of the radial component of residual macrostresses in the noted interval. At the same time, the grouped curves for
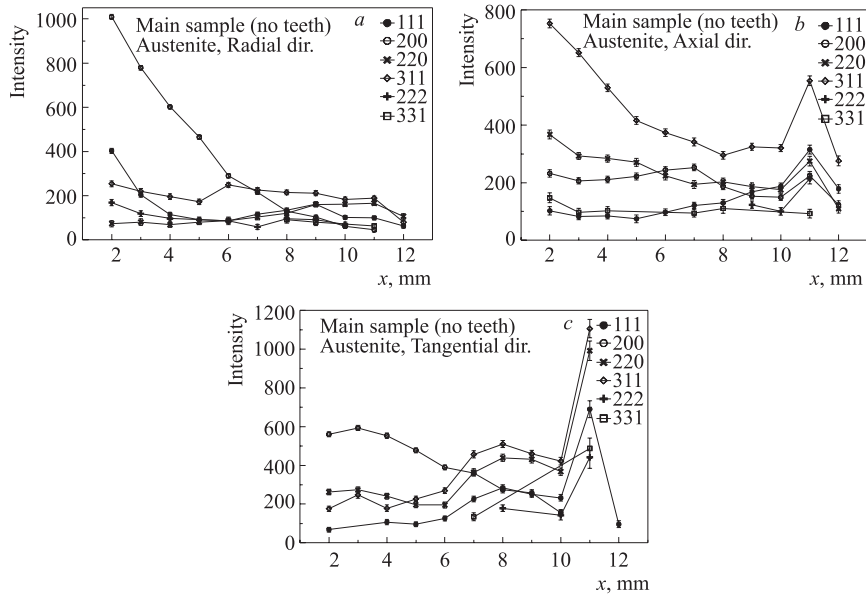
8

Fig. 8. Selected peaks intensities of the austenite phase of the main sample on the location x of the gauge volume in the direction: a – radial, b — axial, c — tangential
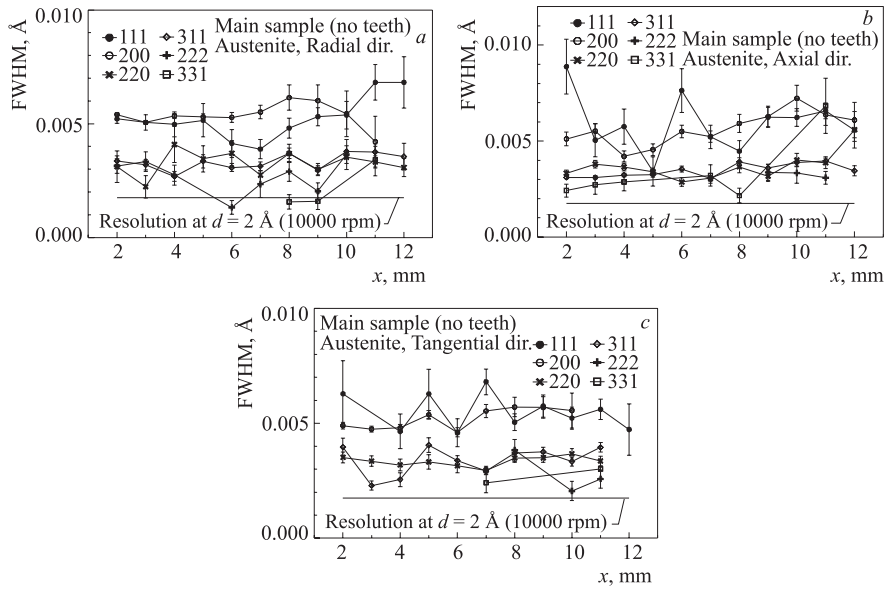

Fig. 9. Selected peaks widths of the austenite phase of the main sample on the location x of the gauge volume in the direction: a — radial, b — axial, c — tangential
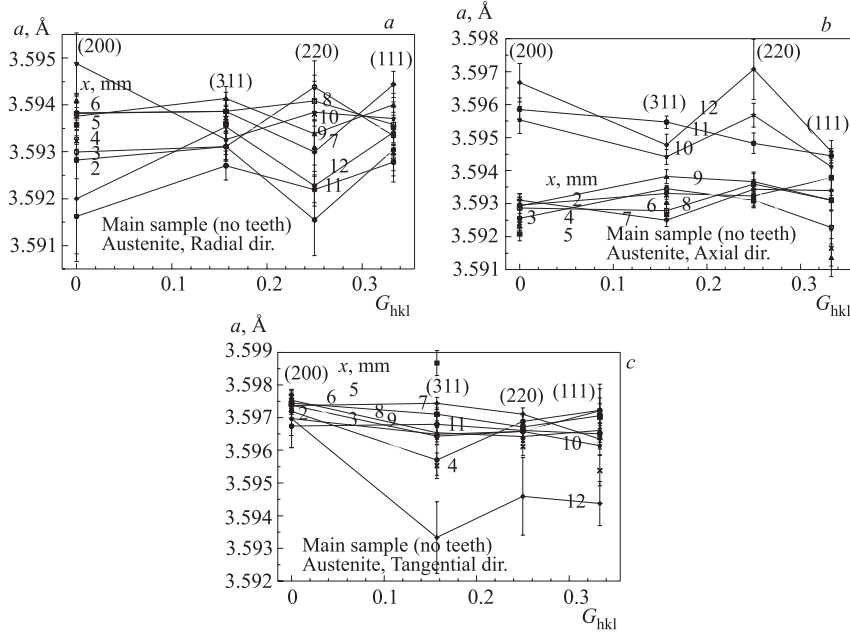
9

Fig. 10. Selected peaks lattice parameters of the austenite phase of the main sample on the anisotropy factor G in the direction: a — radial, b — axial, c — tangential

the axial and tangential directions have distinctly expressed positive and negative slopes that correspond the macroscopic tension and compression, respectively.

Cladding (ferrite). In Figs. 11–14, the same plots are presented for the ferrite phase of the main sample as shown for the austenite phase of the same sample in Figs. 7–10.

The ferrite phase texture and the microstresses of the III type are characterized by Figs. 12 and 13, where the dependences of the selected peaks intensity and width on the location x of the gauge volume are shown for all directions. Variation of the peaks intensity is also rather large as in the austenite phase, especially, in the reflex (211) for all directions. Note that the ferrite peaks width more strongly depends on the coordinate x, than in the austenite phase, increased close to the interface between two phases.

The dependences of the ferrite lattice parameter on the anisotropy factors G are shown in Fig. 14. The ferrite lattice parameters vary nonlinearly as in the austenite phase. This points to the presence of the microstresses of the II type. However, the anisotropy curves grouped in the coordinate interval of $x = 20$–24 mm have on average the small slope for all directions that can point out an absence of the residual macrostresses.
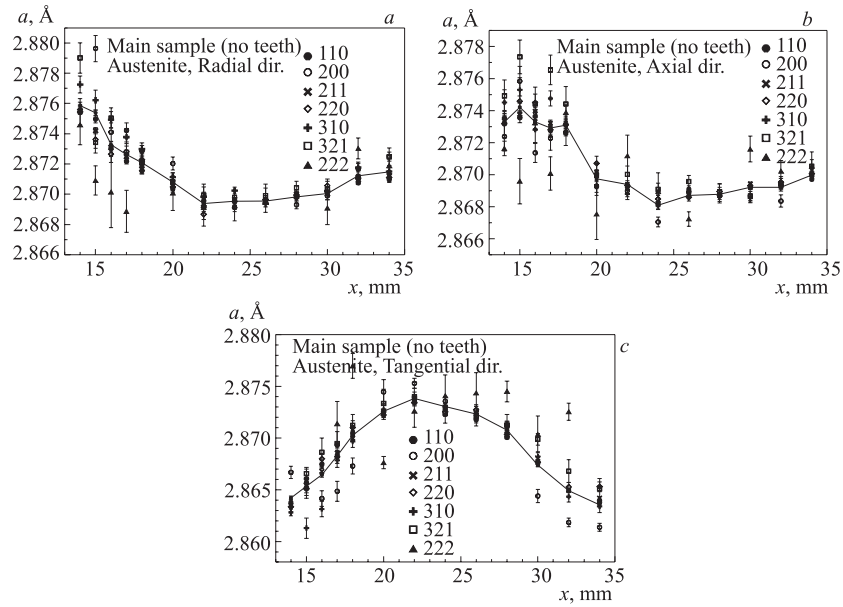
10

Fig. 11. Lattice parameters of the ferrite phase of the main sample on the location x of the gauge volume in the direction: a — radial, b — axial, c — tangential
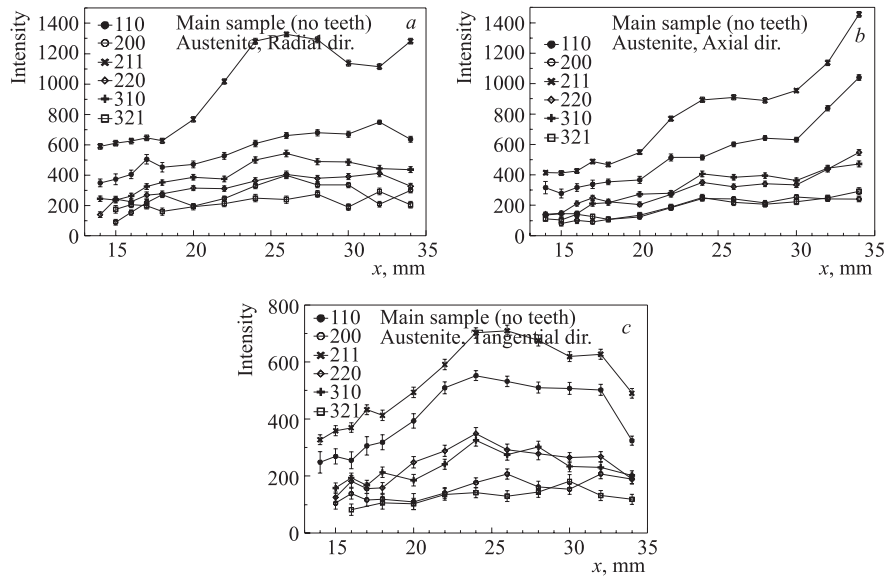

Fig. 12. Selected peaks intensities of the ferrite phase of the main sample on the location x of the gauge volume in the direction: a — radial, b — axial, c — tangential
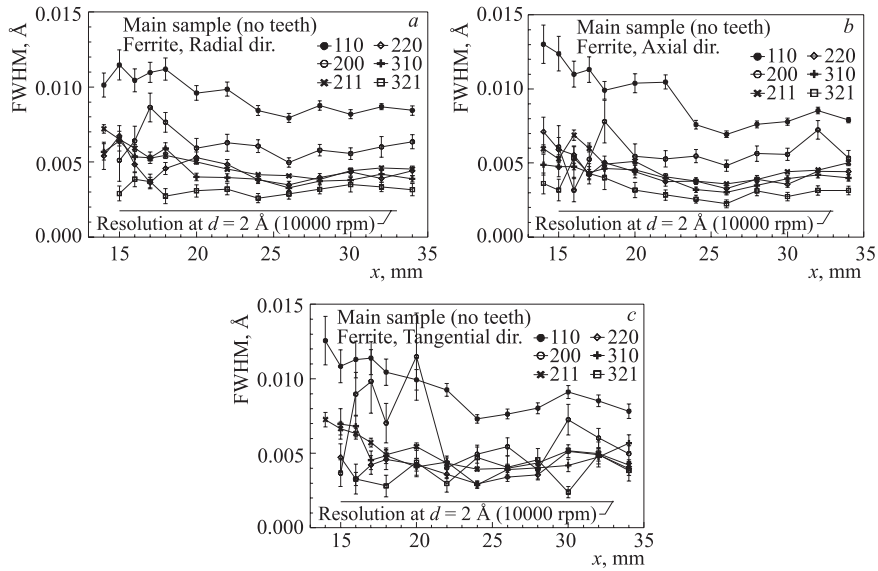
11

Fig. 13. Selected peaks widths of the ferrite phase of the main sample on the location x of the gauge volume in the direction: a — radial, b — axial, c — tangential
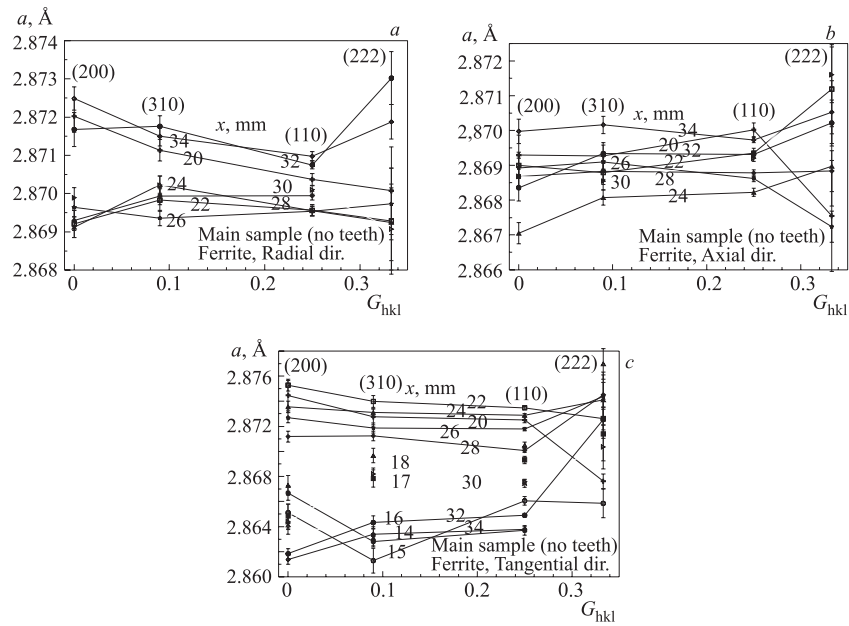

Fig. 14. Selected peaks lattice parameters of the ferrite phase of the main sample on the anisotropy factor G in the direction: a — radial, b — axial, c — tangential

12

The autoindexing lattice parameters of austenite and ferrite phases for all three scattering vector directions are concentrated in Fig. 15.
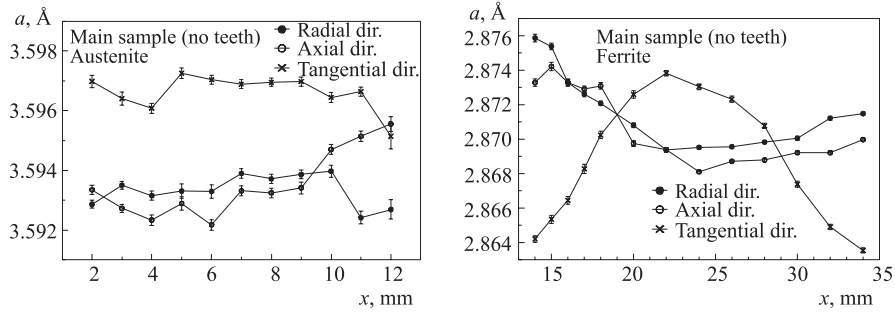

Fig. 15. Phase autoindexing lattice parameters of the main sample on the coordinate x for the radial, axial and tangential directions: left — austenite, right — ferrite

3.2. Comb Sample. Parent tube (austenite). In Figs. 16 and 17, we have presented the dependences of the austenite phase lattice parameter of the comb sample obtained from results of the single peak fitting and the autoindexing. As is seen from Fig. 17 all reflections apart from some peaks show absence of the lattice parameter variation along selected teeth.
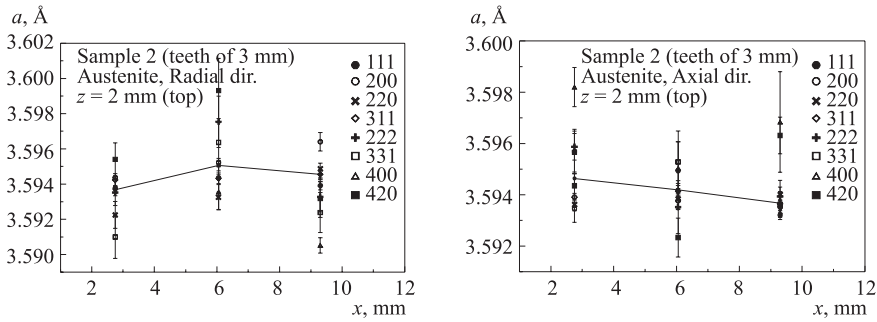

Fig. 16. Selected peaks and autoindexing (solid line) lattice parameters of the austenite phase of the comb sample on the coordinate x at $z = 2$ mm (tooth top) in the direction: left — radial, right — axial

The dependences of the austenite lattice parameter in the teeth tops on the anisotropy factors G are shown in Fig. 18. Although, the austenite lattice parameters vary nonlinearly in both measured directions, on the whole, we can establish that there are a compression (the negative slope) in the radial direction and a
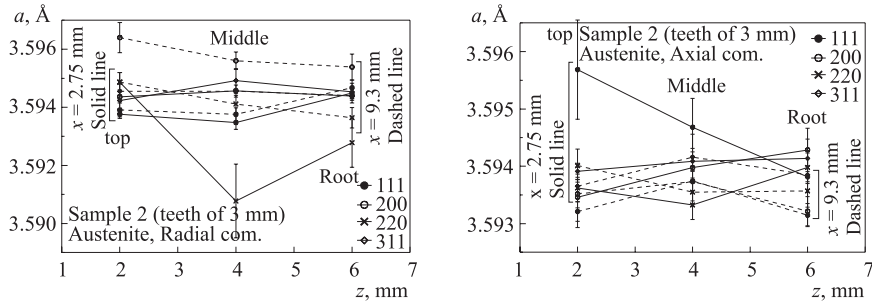
13

Fig. 17. Selected peaks lattice parameters of the austenite phase of the comb sample on the coordinate z at $x = 2.75$ (solid line) and 9.3 mm (dashed line) in the direction: left — radial, right — axial

feeble tension (the positive slope) in the axial direction. This can point to the incomplete relief of the residual macrostresses in the austenite part of the comb sample.
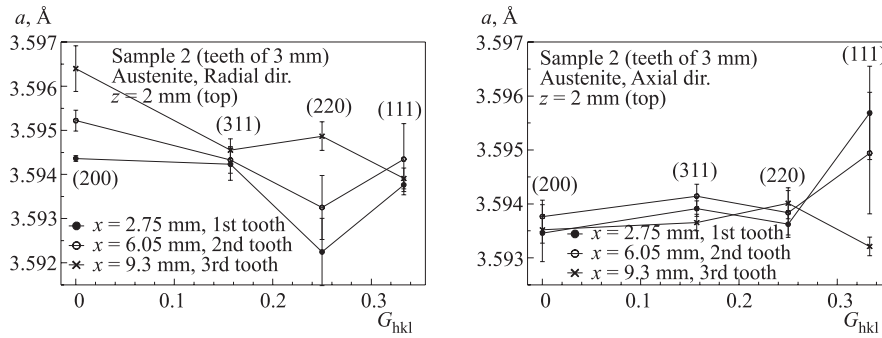

Fig. 18. Selected peaks lattice parameters of the austenite phase in the teeth tops on the anisotropy factor G in the direction: left — radial, right — axial

Cladding (ferrite). In Figs. 19 and 20, we have presented the dependences of the ferrite phase lattice parameter of the comb sample obtained from results of the single peak fitting and the autoindexing.

As in the austenite phase, all ferrite reflections apart from some peaks show absence of the lattice parameter variation along selected teeth.

The dependences of the ferrite lattice parameter in the teeth tops on the anisotropy factors G are shown in Fig. 21. Although, the ferrite lattice parameters vary nonlinearly in both measured directions, on the whole, we can establish that practically there is not a slope in both directions. This can point to the almost
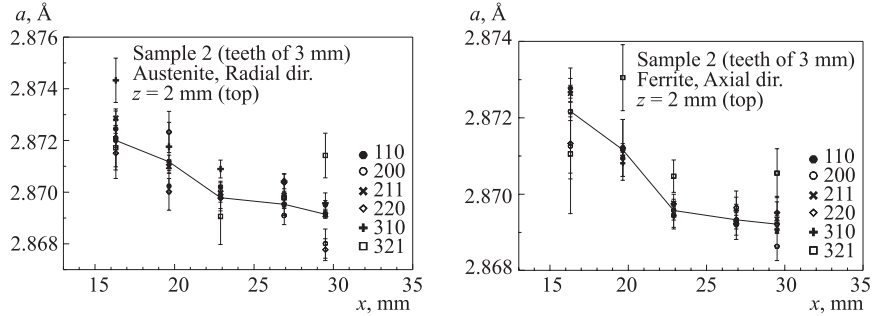
14

Fig. 19. Selected peaks and autoindexing (solid line) lattice parameters of the ferrite phase of the comb sample on the coordinate x in the direction: left — radial, right — axial
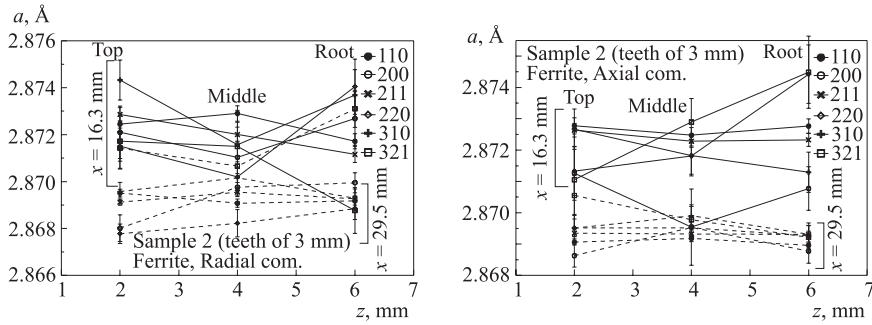

Fig. 20. Selected peaks lattice parameters of the ferrite phase of the comb sample on the coordinate z at $x = 16.3$ (solid line) and 29.5 mm (dashed line) in the direction: left — radial, right — axial
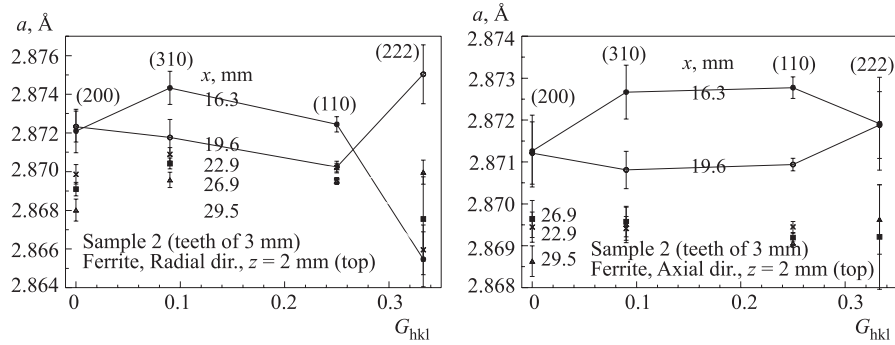

Fig. 21. Selected peaks lattice parameters of the ferrite phase in the teeth tops on the anisotropy factor G in the direction: left — radial, right — axial

15

complete relief of the residual macrostresses in the ferrite part of the comb sample. In the case, the observed x-dependences of the ferrite lattice parameter in the comb sample (Fig. 19) can be put down to the microstresses of II type and (or) a variation of chemical composition of the ferrite phase.

4. EVALUATION OF STRAIN FREE PHASE LATTICE PARAMETERS

Finding the lattice parameter a from the measured spectrum allows the strain ε to be evaluated if the strain fee lattice parameter a_0 is known:

$$\varepsilon = (a - a_0)/a_0. \tag{1}$$

However, in both previous experiments we have encountered with some difficulties in determining the value of these quantities for the α and γ phases. We have tried to determine a_0 using powder samples made from the austenitic steel part of the tube as well as from the welded material. It looked as if these powders did not provide strain free reference states of the tube constituents. Possibly, filling and annealing these materials caused structural changes and falsified the a_0-values, e. g., the martensitic phase could be built during the cold forming process in austenitic steel. In the welded ferritic material the carbon content might change and, as a result, a_0 altered. In such unclear situation, the so-called edge (boundary) values measured far from the interface have been used as strain free lattice parameters. It was based on the proximity of the lattice parameters for all directions of the scattering vector in both phases.

However, an answer to the question whether the use of the edge values of a as a_0 is justified in this situation becomes more difficult because the calculated strain/stress values depend strongly on the deviation of a_0 from the true value in each point of the sample. Another approach was used to process the experimental data obtained on the HRFD instrument [1]. Since the axial component was not measured in the experiment, we were able to calculate only the difference between the radial and tangential components of the strain and stress tensors:

$$\delta\varepsilon_{\mathrm{rad-tan}} = \varepsilon_{\mathrm{rad}} - \varepsilon_{\mathrm{tan}} = (a_{\mathrm{rad}} - a_{\mathrm{tan}})/a_0, \tag{2}$$

$$\delta\sigma_{\mathrm{rad-tan}} = \sigma_{\mathrm{rad}} - \sigma_{\mathrm{tan}} = E\delta\varepsilon_{\mathrm{rad-tan}}/(1 + \nu), \tag{3}$$

where a_{rad} and a_{tan} are the lattice parameters for the radial and tangential directions. The difference value has feeble sensibility to small deviations of a_0 from its true value, consequently, it is convenient to use the values of $\delta\varepsilon$ and (or) $\delta\sigma$ to compare the results of the measurements on the different diffractometers as well as with results of the destructive methods and the finite element calculation. In the case of the POLDI experiment, in which we have measured all three strain

components, there was no necessity to use the noted approach. However, the edge phase lattice parameters are distinguished in the different directions (Figs. 11 and 17), therefore they cannot simply be averaged on the different directions. Other approach is required in this case. To explain it on a concrete example, we have collected the edge phase lattice parameters of the main sample in Table 3.

Table 4. Edge values of autoindexing phase lattice parameters in main sample

Lattice parameter, Å	Austenite phase ($x = 2$ mm)	Ferrite phase ($x = 34$ mm)
a_{rad}	3.59286(13)	2.87148(10)
a_{ax}	3.59335(15)	2.86997(10)
$a_{\mathrm{aver(rad,ax)}}$	3.59310(20)	2.87073(14)
a_{tan}	3.59698(21)	2.86345(15)
$\mathrm{gap}_{\mathrm{(aver,tan)}}$	−0.00382(28)	0.00728(20)

In both phases the edge radial and axial lattice parameters are comparable with each other within the 2–4 experimental errors. However, there is a gap between the averaged parameter $a_{\mathrm{aver(rad,ax)}}$ for these directions and the tangential parameter a_{tan}. This effect can point to existence of the uniaxial stress σ_{tan} along the tangential direction on the edges of the main sample, namely, the tension stress on the inner edge and the compression stress on the outer edge. At that, the perpendicular strain components mainly reflect a contraction and an expansion according to the Poisson ratio in the austenite and ferrite phases, respectively, i. e., they are not caused by additional residual stresses. Accepting this hypothesis and using the Hook low the strain components can be written as follows:

$$\varepsilon_{\mathrm{aver(rad,ax)}} = -\nu\varepsilon_{\mathrm{tan}}, \tag{4}$$

where

$$\varepsilon_{\mathrm{aver(rad,ax)}} = (a_{\mathrm{aver(rad,ax)}} - a_o)/a_o. \tag{5}$$

Then the following formula can be deduced for the strain free lattice parameter:

$$a_0 = (a_{\mathrm{aver(rad,ax)}} + \nu a_{\mathrm{tan}})/(1 + \nu) \tag{6}$$

from which we have obtained $a_0 = 3.59400(18)$ Å for the austenite phase and $a_0 = 2.86905(13)$ Å for the ferrite phase.

Now we pass to an evaluation of the strain free lattice parameter from measurements with the comb sample. In Fig. 22, we have combined results of autoindexing for the main and comb samples in the radial and axial directions. As in the austenite phase of the main sample the lattice parameter of the comb sample very weakly depends on the coordinate x in the interval of $x = 2$–6 mm.

Analyzing of *the austenite phase* (Fig. 22, left) we can note the followng peculiarities of the radial component: 1) the anisotropy analysis of the main sample (Fig. 10, a) has demonstrated a smallness of the radial residual macrostress
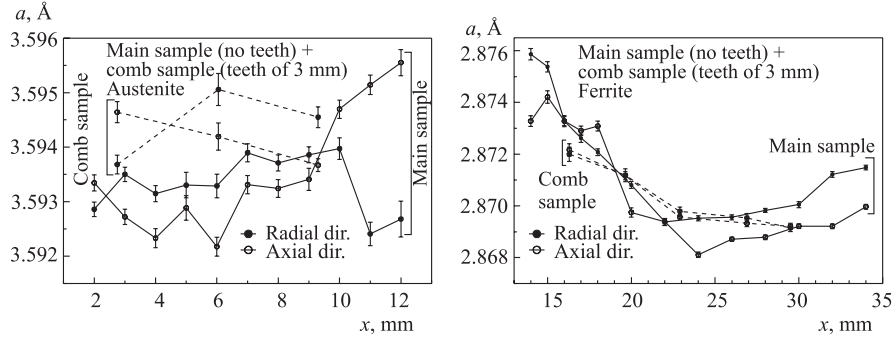
Fig. 22. Autoindexing lattice parameters of the austenite (left) and ferrite (right) phases of the main and comb samples on the coordinate x for the radial and axial directions

component in the coordinate interval of $x = 2$–6 mm; 2) the comb lattice parameter was larger than in the main sample as seen from Fig. 22 (left); 3) the radial residual macrostress component was compressive in the comb sample, as we have shown in Subsec. 3.2 during the anisotropy analysis (Fig. 18, left). The above-mentioned features contradict each other. In fact, the radial residual macrostress component was lacking or small in the main sample but it became compressive in the comb sample, i. e., the lattice parameter has to be decreased. However, the measurements show the opposite, i. e., the lattice parameter is increased. In the same manner as for the radial component of the austenite we list features of the axial component behavior: 1) the anisotropy analysis showed that the axial residual macrostress component in the main sample was tensile in the coordinate interval of $x = 2$–6 mm (Fig. 10, b); 2) the comb lattice parameter was larger than in the main sample; 3) the axial residual macrostress component in the comb sample was close to zero or feeble tensile as we have shown in Subsec. 3.2 during the anisotropy analysis (Fig. 18, c). Similarly to the radial component the noted features of the axial component contradict each other.

It is possible to offer two explanations to the noted contradictions in the austenite phase. First one consists in occurrence of the additional residual stresses in the comb sample after the EDM cutting. But this question was specially studied during the *in-situ* EDM testing experiment on the ENGIN-X instrument [8]. The high elastic thermal strains were directly observed at the time of working of the EDM apparatus but any additional residual stresses were not fixed after a sample cooling. Other explanation consists in various geometrical configurations of the main and comb samples that could be resulted in redistribution of the residual stresses. And though we had the sample No. 3 (Fig. 3, top right) with the same

18

configuration that the used comb sample No. 2 but it was not measured due to lack of the beam time.

As we noted early, the presence of the residual stresses of I type (i.e. macrostress) in the comb sample can point out their incomplete relief. It is possible that the created artificial comb structure is too rough. Remind that the size of the teeth in the axial direction was equal to 10 mm. It would be useful to perform the measurements with modified comb sample in which the teeth of the 3×3 mm^2 cross section will be done by the additional EDM cutting slits along the radial direction.

Finishing discussion of the austenite phase, the only decision, which we can accept in these circumstances, consists in averaging of the comb lattice parameters for both directions in the coordinate interval of $x = 2$–6 mm and using the obtained value of 3.59439(59) as the stress free austenite reference. The last value is comparable with 3.59400(18) calculated using the edge uniaxial stress hypothesis.

Now we shall consider a situation with *the ferrite phase* (Fig. 22, right). The ferrite phase plot differs much from similar one for the austenite phase. Above all, we shall note a vicinity of the x dependences of the ferrite lattice parameter for the main and comb samples in both directions excepting the intended tendency to a divergence of these dependences close to the interface and the outer edge. Secondly, the lattice parameter appreciably varies along the tube radius. Thirdly, the ferrite anisotropy analysis has shown that, on the whole, the main (Fig. 14) and comb (Fig. 21) samples were weakly and approximately equally deformed in the radial and axial directions.

Listed facts, especially the last one, give a ground to employ the uniaxial stress hypothesis to the whole of the ferrite part of the main sample. The results of calculation of a «stress free» lattice parameter are shown in Fig. 23 in comparison with the experimental results of the comb sample. A startling coincidence of the curves can serve as a forcible argument in favor of a reallocation of the chemical composition in the ferrite part of the composite tube during weld overlaying, especially, carbon content. But it is a circumstantial argument. Only an experimental observation of similar dependence in the comb sample for the tangential direction which is brightly expressed in the main sample could be served as a direct proof of the chemical hypothesis. In this connection it would be desirable to continue measurements with the comb sample No. 2 (teeth of 3 mm width) to reconstruct the triaxial map of the residual stress tensor as well as measurements with the comb sample No. 1 (teeth of 1.5 mm width) to check effect of a tooth width.

Within the framework of the chemical reallocation hypothesis the practical absence of change of the lattice parameter along the teeth (Fig. 20) can quite be explained as the tooth axis was directed along the tangential direction in which a change of the chemical composition was not expected. Note that the chemical
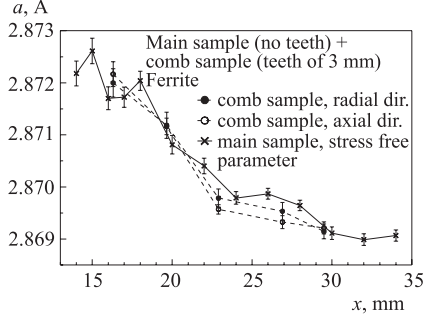
19

Fig. 23. Ferrite lattice parameters of the comb sample in comparison with the stress free parameters calculated by using of the uniaxial stress hypothesis for the main sample
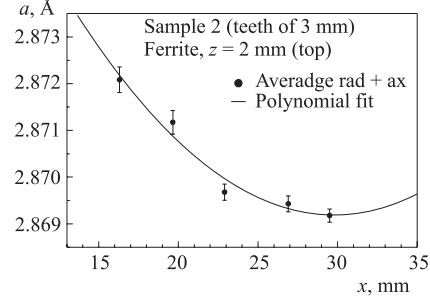
Fig. 24. Average ferrite lattice parameters of the comb sample and a polynomial fit of the 3rd degree of the experimental curve

reallocation hypothesis has to lead to nullification of any contribution of chemical origin in the difference of two any components of the strain and stress tensors. In this light, it has become clear why a qualitative agreement between the ND experimental difference of the radial and tangential stress components and the corresponding TOM and FEM results was observed in [1, 2].

Considering stated reasons we used the following approach to the estimation of the stress free lattice parameter a_0 in the ferrite phase. The experimental results of the comb sample were averaged on both directions and approximated by a polynomial of the 3rd degree (Fig. 24). To obtain a_0 for the ferrite phase, we have interpolated the polynomial fit on the unmeasured radius intervals. In particular, the interpolated to $x = 34$ mm value of a_0 has appeared equal 2.86948 that is rather close to 2.86905 (13) obtained within the framework of the edge uniaxial stress hypothesis. Thus, as a radial dependence of the stress free lattice parameter for the ferrite phase we have used a function of $a_0(x) = 2.883789 - 0.000981x + 1.647E - 05x^2$.

5. STRAIN/STRESS CALCULATION

As we have mentioned in Sec. 4, the difference $\delta\varepsilon_{i-j}$ of any two components of the strain tensor has feeble sensibility to small deviations of a_0 from its true value, consequently, it is convenient to use the value of $\delta\varepsilon_{i-j}$ to compare the results of the measurements on the different stress-diffractometers. The results of the HRFD, ENGIN and POLDI experiments for the difference $\delta\varepsilon_{\mathrm{rad-tan}}$ of radial and tangential components are shown in Fig. 25. The distinction of results of the

last experiment from the two previous ones is obvious. This distinction can be related on different geometry of the investigated samples cut out from the 70° circumference segment by various ways.
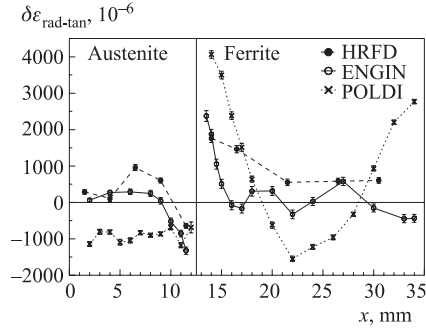

Fig. 25. Difference $\delta\varepsilon_{\mathrm{rad-tan}}$ of radial and tangential components of the strain tensor from the HRFD, ENGIN and POLDI experiments
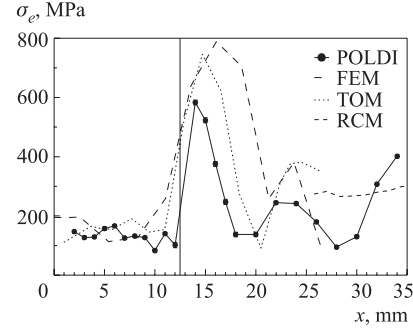
Fig. 26. Comparison of the von Mises equivalent stresses σ_e calculated from the POLDI (noncorrected), FEM, TOM and RCM results

To compare the ND results with the TOM, RCM and FEM results we have used a very effective approach based on calculation of the von Mises equivalent stress σ_e

$$\sigma_e = \sqrt{\frac{1}{2}\left[(\sigma_{rad} - \sigma_{ax})^2 + (\sigma_{rad} - \sigma_{\tan})^2 + (\sigma_{ax} - \sigma_{\tan})^2\right]} \qquad (7)$$

that includes all possible pairwise stress differences σ_i–σ_j, where i and j correspond to a pair of any scattering vector directions ($i \neq j$). Note that the von Mises stress is independent of a hydrostatic stress component as well as of possible non-uniform redistribution of the chemical composition during the welding process, e. g., fixed carbon, and connected to it the stress free lattice parameter change along radius of the tube, especially, in the cladding. A weak sensibility of the von Mises stress to small deviations of a_0 from its true value is quite obvious out of Eqs. (2)–(3). The results of the equivalent stress calculation are shown in Fig. 26. The qualitative agreement of the results of all four used methods may be stated.

Absolute values of the stress tensor components from the POLDI data were calculated within the framework of the elastic model approximation:

$$\sigma_i = \frac{E}{1 + \nu}\left[\varepsilon_i + \frac{\nu}{1 - 2\nu}(\varepsilon_{rad} + \varepsilon_{ax} + \varepsilon_{\tan})\right]. \qquad (8)$$

21

For this calculation it is critically important to use the best approximation of the parameter a_0 to a true stress free lattice parameter. In Sec. 4, we have noted three possible approaches for the evaluation of a_0: 1) use of the uniaxial stress hypothesis initiated by presence of the gap between the lattice parameters in the different directions on the tube edges; 2) application of this hypothesis to any whole phase part of the main sample; 3) use of the averaged results of measurements in the radial and axial directions with the comb sample. We have tested all three approaches of evaluation of a_0 during the stress calculations. The results of use of the third approach are shown in Figs. 27 and 28 in comparison with the TOM and FEM results.
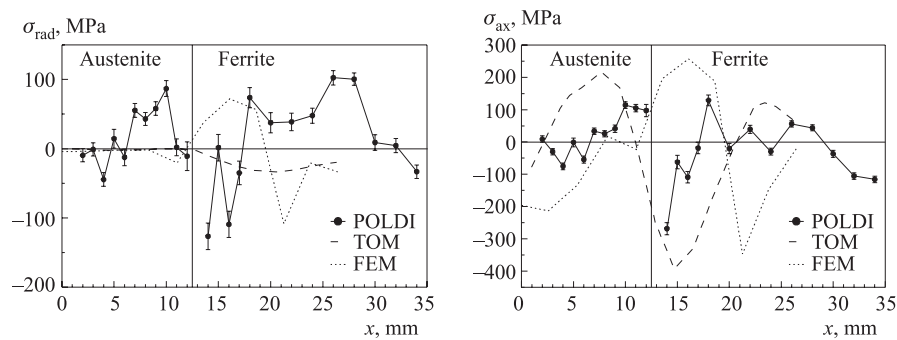

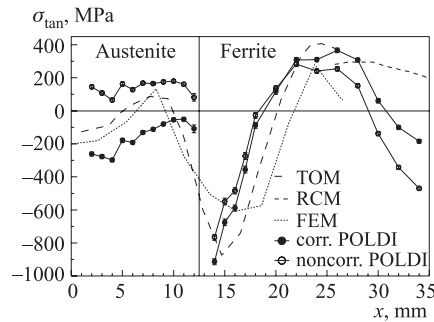Fig. 27. Residual stresses in the main sample in the direction: left — radial, right — axial

Fig. 28. Residual stresses in the main sample on the coordinate x for the tangential direction

As the ND data were obtained for a small part of the tube they have to be corrected for the stress released during the cutting procedure (see Table 2). Assuming that the released stress varied linearly over the interval from the outer to the inner edge of the tube and that the radial component did not change essentially during cutting, the residual stress in the uncut tube can be predicted from the ND

22

data. The corrected POLDI results for the tangential direction are presented in Fig. 28. The results in the austenite phase had the greatest correction. But the same correction has not introduced the principal changes in the ferrite phase. The POLDI results shown in Fig. 27 were not corrected for the stress relieve as the correction was insignificant.

6. DISCUSSION

Figure 27 demonstrates a contradictory picture between the experimental and calculated data for the radial and axial directions. The presented methods have shown results for the radial direction completely contradicting each other. The similar picture is observed for the axial direction though the POLDI and TOM results are not in the too rough contradiction. Note that the TOM and FEM curves for the axial direction are shifted onto about 5–6 mm, at that, the peak values of the axial stresses are nearly equal. As to the radial stress component obtained by the TOM, it was not directly determined, but calculated from a condition of the forces balance with use of the TOM results for two other stress components. Only for the tangential direction (Fig. 28) we can establish a qualitative agreement of the results of all presented methods, especially, for the ferritic phase. For the austenitic phase, some disagreement is certainly related to the uncontrollable influence of microstresses of the II type on the results of ND measurements. As is visible from Fig. 28, the cladding produced the compressive stress of about 800 MPa on the austenitic tube that can prevent stress corrosion in service.

The comparison of the curves in Fig. 27 with the curves in Fig. 28 clearly shows a reason of the qualitative agreement of calculation results of the difference of the radial and tangential stress components $\delta\sigma_{\mathrm{rad-tan}}$ and the von Mises equivalent stress σ_e from the POLDI results with the FEM and TOM results. Really, the tangential stress component prevails over two others, namely, for it we have noticed the qualitative agreement of all methods with each other (Fig. 28).

7. CONCLUSIONS

The present study has demonstrated the application of the time-of-flight neutron diffraction realized on the POLDI stress-diffractometer at the SINQ spallation source to measure the triaxial residual stresses in the composite tube from austenitic stainless steel with welded ferritic steel cladding fabricated by the welding overlaying technique. The objective of this research was to collect experimental information that can be helpful for the optimization of the welding technique.

The investigated sample was cut from the composite tube as a thin 70° circumference segment by thickness of 10 mm. The strain scanning was performed

along the tube radius through the austenite and ferrite phases with three mutually perpendicular directions of the neutron scattering vector: radial, axial and tangential. The neutron diffraction pattern was analyzed by the single peak fit and autoindexing programs to determine a phase lattice parameter.

The comb sample with teeth of 3 mm width machined by EDM from the tube was investigated to evaluate the stress free lattice parameter a_0 for the residual strain/stress calculations. Though only the radial and axial strain components were measured in the comb sample, nevertheless the clear indication on the radial dependence of the stress free lattice parameter a_0 was obtained. We attribute this dependence to non-uniform redistribution of the chemical composition during the welding process, namely, fixed carbon.

Using the comb-sample lattice parameter results the triaxial residual stresses were revealed in the composite tube. The necessary correction was introduced into the axial and tangential stress components as only they were controlled during the sample cutting procedure. Comparison of the stress results from the ND measurements with the FEM, RCM and TOM results has shown that there was a semiquantitative agreement among all of the used methods only for the tangential direction. For two other stress components the contradictions between these methods were rather strong, especially, for a rather weak radial component.

The strong compressive tangential residual stress of about 800 MPa was observed in the ferrite cladding close to the interface between the parent tube and the cladding. At that, the cladding has created the smaller on value but quite appreciable tangential compressive stress in the austenite phase which can prevent stress corrosion of the tube in service.

REFERENCES

1. *Taran Yu. V., Schreiber J., Mikula P., Lukas P., Vrana M., Bokuchava G. D., Kockelmann H.* Neutron diffraction measurements of residual stress in an austenitic steel tube with a welded ferritic cover. // Proc. of the 4th European Conf. of Residual Stresses, Cluny, France, June 1996. P. 87–95.

2. *Kockelmann H., Schreiber J., Taran Yu. V., Wright J. S.* Investigation of residual stresses in a shape welded steel tube by the time-of-flight neutron diffraction technique // Materials Science Forum. 1999. V. 321–324. P. 726–731.

3. *Berreth K., Kockelmann H.* Optimierung der Formschweißtechnik für druckführende und korrosiv beanspruchte Komponenten der chemischen Industrie. Abschlußbericht zum Forschungsvorhaben AiF-Nr. 8954. MPA, Universität Stuttgart, 1995.

4. *May P. S., Wimpory R. C., Webster G. A., O'Down N. P.* Determination of the residual stress distribution in a welded T-plate joint. The Annual Report 2000 of Studsvik Neutron Research Laboratory. REST Experimental Report No. 425; http://www.studsvik.un.se/Publications/AnnualReports/Ar00/425.pdf.

5. *Wimpory R. C., May P. S., O'Down N. P., Webster G. A., Smith D. J., Kingston E.* Measurement of residual stresses in T-plate weldments // J. Strain Analysis for Engineering Design. 2003. V. 38. P. 349–365.

6. *Hughes D. J., James M. N., Hattingh D. G., Webster P. J.* The use of combs for evaluation of strain-free references for residual strain measurements by neutron and synchrotron X-ray diffraction // J. Neutron Researches. 2003. V. 11. P. 289–293.

7. *Zlokazov V. B.* AUTOX – A program for autoindexing reflections from multiphase polycrystals // Comp. Phys. Commun. 1995. V. 85. P. 415–422.

8. *Truman C. E., Smith D. J., Kingston E.* Following engineering processes in-situ: stresses due to electro-discharge machining. The ISIS Annual Report 2005. RAL-TR-2005-050, Didcot, 2005. P. 16.